Enhancing Optical Confinement of InGaN Thin-Film Microdisk Lasers with Hybrid Omnidirectional Reflectors

Zhongqi Wang, Yuk Fai Cheung, Wai Yuen Fu, and Hoi Wai Choi*

Department of Electrical and Electronic Engineering, The University of Hong Kong, Hong Kong 999077, China

E-mail: hwchoi@hku.hk

Accepted Manuscript (doi: 10.1021/acsphotonics.4c00132)

Abstract

The conventional GaN microdisk laser adopts an undercut structure for the optical confinement, which provides poor overlap between the whispering gallery modes and the multiquantum well gain region. The thin-film microdisk structure was proposed to overcome this shortcoming, but the absorptive nature of the metallic bonding layer with mirror compromises optical confinement. In this work, an SiO_2/TiO_2 distributed Bragg reflector is integrated with the metallic mirror to form an omnidirectional reflector that provides high optical reflectance across a wide range of incidence angles to promote optical confinement in the microdisk. Optical-pumped lasing with an average lasing threshold power density of 46.5 W/cm^2 and Q factors of 18200 (near threshold) is achieved. The narrowest lasing line width of ∼0.02 nm is obtained at the average excitation power density of 48.02 W/cm^2, representing a major advancement in the GaN microdisk laser technology.

Introduction

GaN-based devices are widely found in a diverse range of optoelectronic and electronic applications including lighting, display, optical storage, and power supplies. With growing demand for ultraviolet–visible light laser diodes for current and upcoming applications, such as laser lighting, LiDAR, and visible-light communications (VLC), research on GaN-based lasers has constantly been gaining momentum. Among them, the GaN-based microdisk lasers have drawn significant interest due to their wide wavelength coverage, high optical gain, small modal volume, uncomplicated structure, and simple fabrication process.[1] The low-loss characteristics of an ideal microdisk laser at the cavity boundary, where total internal reflection (TIR) occurs, result in higher optical finesse and lower lasing thresholds.

In the design of microdisk structures, the primary focus lies on their optical confinement ability and the overlap factor between the whispering gallery modes (WGMs) and the gain region. The lateral optical confinement in the cavity is achieved by confining light in the circular high refractive index GaN microdisk achieve TIR at the cavity boundary.[2–4] As for vertical confinement, the most common approach is to expose the upper and lower surfaces of the GaN microdisk to air to confine light via the large refractive index contrast.[5–14] However, to expose the bottom surface of the GaN microdisk to form the undercut structure, the material underneath the GaN layer needs to be removed by selective etching. This implies that GaN microdisks with an undercut structure are typically thick (as thick as the entire epitaxial structure which are often in excess of a few microns) resulting in low overlap factors,[15,16] and suffer from a rough bottom surface resulting from selective wet etching,[5,6,9] which could significantly reduce optical confinement. Furthermore, the mechanical stability of such a suspended structure is compromised, and it faces challenges with heat sinking, leading to performance instabilities.

To address these issues, thin-film GaN microdisks have been developed utilizing wafer bonding, substrate removal, and thinning techniques,[10,17–20] enabling optimization of the microdisk thickness without altering the growth process to maintain the high internal quantum

efficiency (IQE) of InGaN/GaN multiquantum wells (MQWs). In this approach, the metallic bonding layer serves as the bottom mirror to provide optical confinement for the microdisks. However, compared to the undercut structure, the lasing threshold and Q factor of these thin-film microdisks with metallic mirrors did not improve significantly due to strong optical absorption of the metal.[18] A previous study explored the utilization of epitaxial 25-pair AlN/AlGaN distributed Bragg reflector (DBR) instead of the undercut structure to achieve optical isolation from the substrate, realizing an optical-pumped ultraviolet GaN microdisk laser with a Q factor of approximately 400.[21] Furthermore, due to the angular dependency of DBR reflection, especially when applied to cavities of high refractive index materials, the reflectance drops sharply as the angle of incidence increases, making it challenging to achieve omnidirectional high reflectivity which is needed for microdisks. While the reflectance and angular range may increase with an increasing number of pairs, thicker DBRs would directly lead to failures in the wafer bonding process. To realize high-quality thin-film GaN microdisk lasers with superior optical isolation from the substrate, an incidental solution presents itself through the incorporation of several pairs of DBR between the high refractive index material cavity and the metallic layer which is needed for the wafer bonding process. This configuration could provide high reflectivity with low absorption losses across a large angular range of the cavity.

Design of the Hybrid ODR Structure

The undercutting technique is one of the most common methods of fabricating microdisk lasers, relying on TIR at the semiconductor–air interface. This is rightly so, as evident from the simulated angular reflectivity plots in Figure 1 for TE polarized light, given that light emitted from InGaN/GaN MQWs is predominantly TE polarized owing to its inherent polarization selective emission characteristics.[22] The finite-difference time-domain (FDTD) simulations are conducted using the Lumerical FDTD software. The reflectivity for the

undercut structure remains high at large angles of incidence but drops sharply when the incident angle is lower than the critical angle. However, it is reflectance at large angles of incidence that contributes to lateral optical confinement in microdisks. In fact, the reduced reflectance at small angles may actually prevent the buildup of vertical modes that competes with the WGMs.

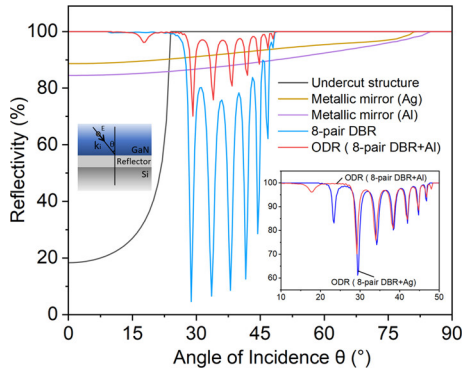

Figure 1: Simulated reflectivity at $\lambda = 450$ nm versus angle for a TE-polarized plane wave by 2D-FDTD simulations. The inset shows the simulated reflectivity for different ODR schemes.

Nevertheless, the limitations of the undercut microdisk as described in the introductory section prompted the development of thin-film microdisk lasers that improve overlap between the WGMs and the gain region. However, the Ag or Al metallic bonding layer, which also serves as the reflector, suffers from reduced reflectivity as shown in the reflectivity plots of Figure 1 due to strong absorption across a wide range of angles, affecting optical confinement in the microdisk. This shortcoming calls for the design of an alternative reflector, with DBR being an obvious choice. As seen in the plot of Figure 1, the 8-pair SiO_2/TiO_2 DBR structure provides nearly 100% reflectivity either at low angles or above the critical angle, although reflectivity is significantly reduced at angles between $\sim 30°$ and $\sim 50°$. The DBR is combined with a metallic layer to form an ODR as required for the bonding process, whose reflectivity remains high over a wide range of angles of incidence, making it an ideal choice for thin-film microdisks.

To validate the effectiveness of this hybrid ODR in a microdisk structure, 3D-FDTD simulations are performed to compare optical confinement in 8 μm diameter thin-film mi-

crodisks with either Ag mirror or the hybrid ODR as the bottom reflector. Both models are simulated with no gain material to capture the resonant modes of the cold cavity. Three orthogonal dipole sources are placed at the edge of the microdisk to stimulate resonant modes. Time monitors were used to observe the field decay of the resonant modes, and profile monitors were used to collect the field patterns of the resonant modes. Identical settings are applied to both simulation models, the only difference being the reflector structure beneath the microdisks of either an Ag layer or the hybrid-ODR. Further details of the simulation models are presented in Supporting Information section 1. Under such conditions, the intensities of the electric field profiles of WGM modes on the same order from the two models, depicted in Figure 2, can be compared to assess the differences in light confinement capabilities. The mode field distribution is weaker in the Ag-confined microdisk due to faster leakage of modes from the microdisk, as Ag has higher optical absorption losses in the blue regime. When injecting the same amount of energy into Ag-confined and ODR-confined microdisks and removing transient effects, the total electric field intensity in the ODR-confined microdisk for the same order WGM is about five times that in the Ag-confined microdisk. The transient signals (see Figure S1) from both models show that the signal decays faster in the Ag-confined microdisk, while part of the energy remains in the cavity modes in the ODR-confined microdisk. The overlap factor, estimated from the ratio of the electric field strength in the MQW region to the total electric field strength in the entire region from the cross-sectional electric field profile, is $\sim$47% for the microdisk with the hybrid ODR, compared to $\sim$43% for the microdisk with the Ag mirror. The enhanced optical confinement and overlap factor promise a larger proportion of emitted light coupling into lasing modes and thus a microdisk laser with higher Q factors.

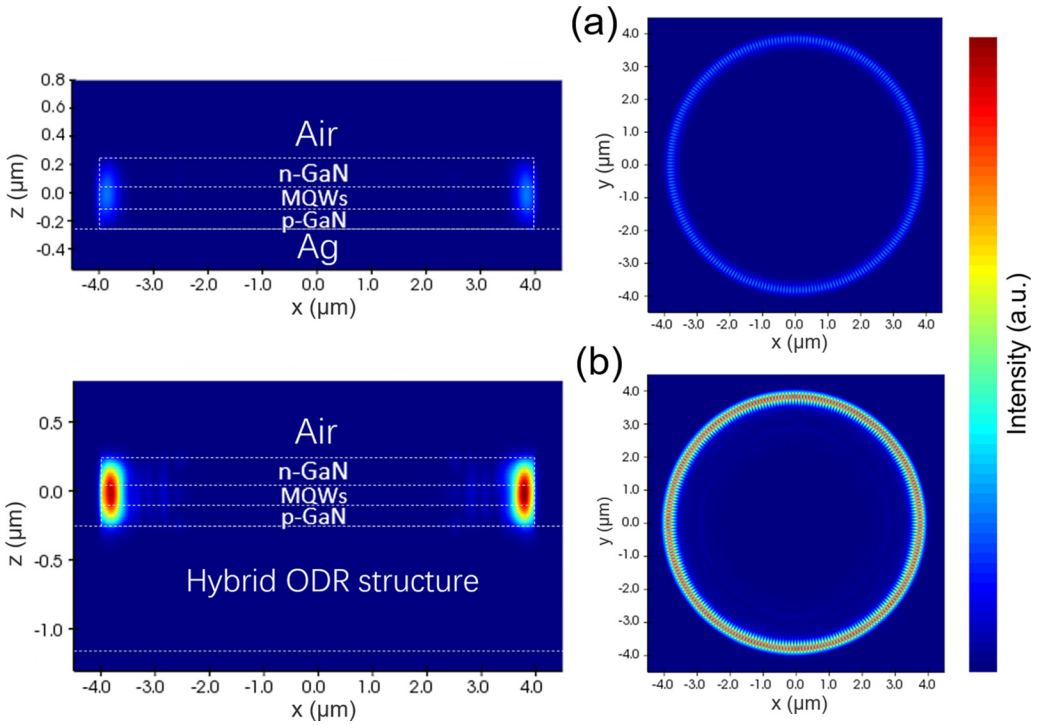

Figure 2: Electric field profiles (using the same intensity color bar scale) from 3D FDTD simulations of 8 μm thin-film microdisks (a) with metallic mirror and (b) with hybrid ODR structure in the cross-sectional view (left) and in the top-view (right).

Experimental Methods

The microdisks are fabricated on blue-light-emitting diode (LED) wafers as depicted in Figure 3a. The wafers are grown by metal–organic chemical vapor deposition (MOCVD) on silicon substrates, with epitaxial structures comprising a 1500 nm-thick AlGaN buffer layer, a 1500 nm-thick n-GaN layer, 150 nm-thick InGaN/GaN MQWs, and a 150 nm-thick p-GaN layer. The device fabrication begins with the hybrid ODR structure. The 8 pairs of SiO_2/TiO_2 (50 nm/80 nm) dielectric DBR[23,24] are deposited on the p-GaN surface of a GaN LED wafer on the Si substrate, followed by annealing at 800 °C for 1 h in an air environment, as indicated in Figure 3b. The Ti/Al/Ti/Au (5 nm/100 nm/25 nm/50 nm) layers are then deposited onto the DBR by e-beam evaporation to form the hybrid ODR as shown in Figure 3c, which also serves as a seeding layer for the electroplating of Cu–Sn for wafer bonding. The sample is then wafer-bonded to a Si substrate, corresponding to

Figure 3d. Wet etch process is then carried out to remove the Si substrate from the GaN LED wafer, as depicted in Figure 3e, after protecting the Si carrier substrate by wax. The exposed GaN surface is further thinned down to about 500 nm by BCl_3-based inductively coupled plasma (ICP) etching as presented in Figure 3f; fabrication of microdisks on such thin-films ensures optimal overlap between optical modes and gain regions. The microdisk patterns are defined by the microsphere lithography (see Figure S3): silica spheres suspended in DI water with diameters of about 8 μm are spin-coated onto the sample (see Figure 3g), followed by ICP etching for the pattern transfer (see Figure 3h). After removal of the residual microspheres by sonication in DI water, the fabrication of microdisks is completed, as illustrated in Figure 3i.

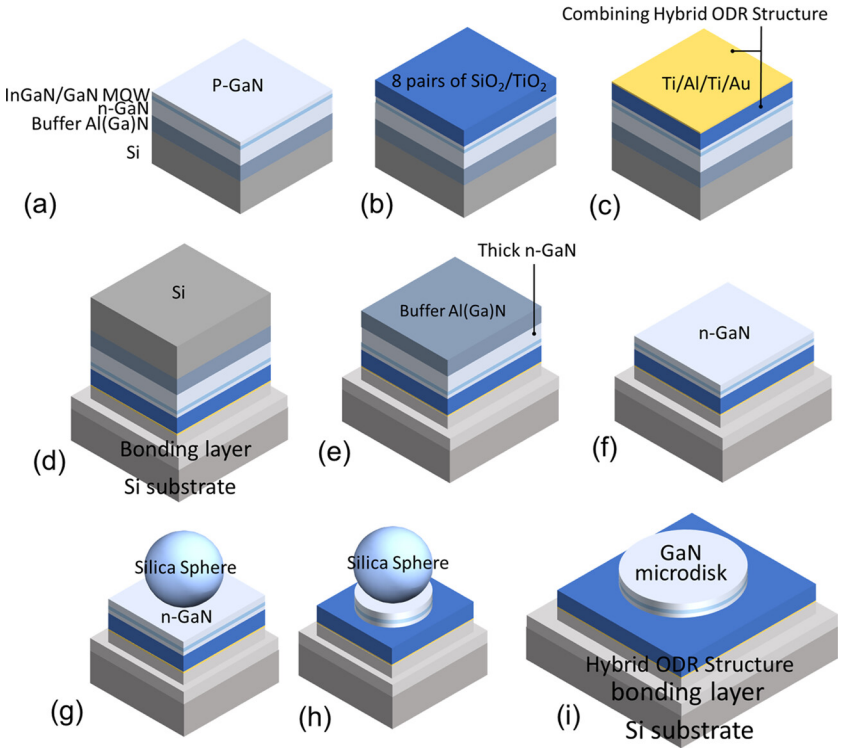

Figure 3: Schematic diagrams illustrating the fabrication steps. (a) As-grown. (b) DBR deposition and annealing. (c) Ti/Al/Ti/Au deposition. (d) Wafer bonding on Si substrate. (e) Si detachment by wet etching. (f) Structure thinned down by ICP etching. (g) Microsphere spin coating. (h) Pattern transfer by ICP etching. (i) Microspheres removed by sonication.

The configuration of a microdisk is shown in Figure 4a, while top and side view SEM images of the fabricated structure are shown in Figure 4b,c, respectively.

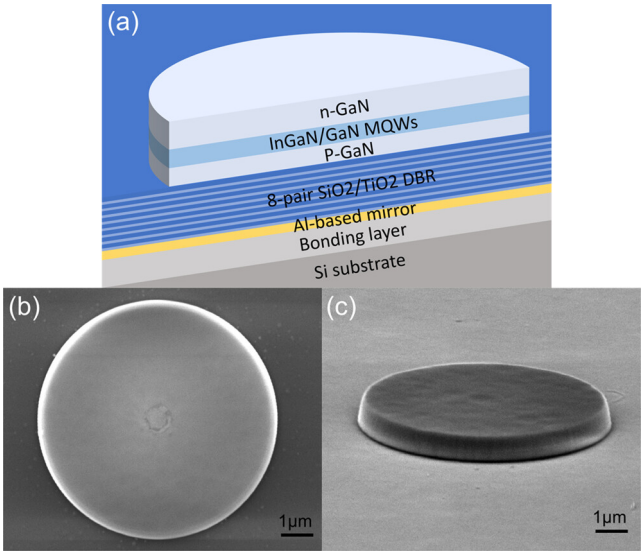

Figure 4: (a) Cross-sectional schematic diagram and SEM images of a thin-film GaN microdisk with the underlying hybrid ODR structure: (b) side view and (c) top view.

Results and Discussion

To investigate the lasing characteristics of these thin-film GaN microdisks with hybrid ODR, room temperature micro-photoluminescence (μ-PL) spectroscopy is conducted using a TUN-TiA-393–408 CNI pulsed laser at a wavelength of 393 nm, a repetition frequency of 50 kHz, and a pulse width of 29.25 ns to pump the microdisk via a 10× microscope objective with a numerical aperture of 0.3 in the normal direction. The μ-PL signals are collected by an optical fiber bundle placed 1 cm away from the sample at an inclination angle of approximately 20°. These optical signals are then coupled to a Horiba iHR-550 spectrograph, dispersed by a 2400 g/mm grating, and detected by a Syncerity BI UV–vis deep-cooled charge-coupled device (CCD). Details of the μ-PL measurement setup are presented in Figure S4. The measured μ-PL spectra at increasing excitation power densities from 44.07 to 60.6 W/cm^2 are illustrated in Figure 5. It is observed that as the excitation power increases, a single spectral peak appears at the center wavelength of 449.96 nm, whose intensity grows rapidly with increasing excitation powers.

Figure 6 plots the integrated intensity and the full width at half-maximum (fwhm) spectral line width of this optical mode as a function of the excitation power density. The PL

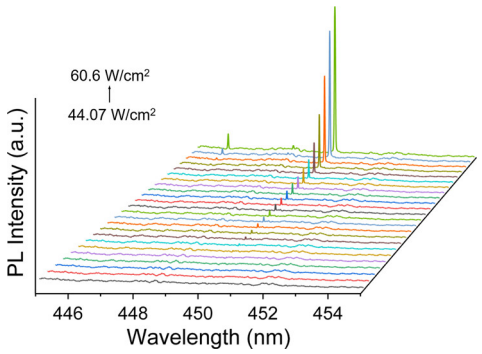

Figure 5: Room-temperature (RT) μ-PL spectra for a thin-film GaN microdisk with a hybrid ODR structure under increasing excitation power density.

intensity rises nonlinearly beyond the lasing threshold (P_{th}) of 46.5 W/cm^2 (corresponding to a peak threshold power 31.8 kW/cm^2) as determined from the distinctive S-shaped input–output curve.

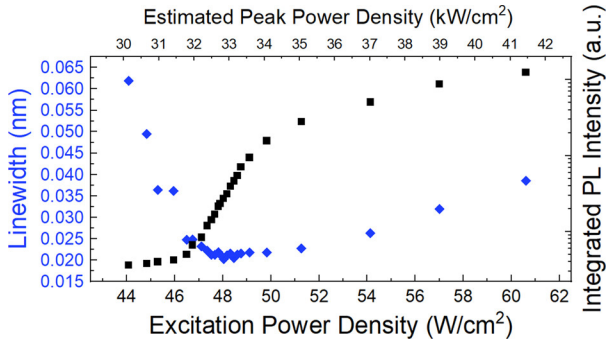

Figure 6: Integrated PL intensities (log scale) vs. excitation power density (black) and spectral width trend (blue). The power meter measures average power (lower x-axis); estimated peak pump power is shown on the upper x-axis.

For a clearer view of the distinctive features of individual spectra, Figure 7 plots the Y-offset-normalized μ-PL spectra at several excitation powers below and above the threshold. When the excitation power is just below the threshold ($\sim$46.48 W/cm^2), the spectral line width is evaluated to be 0.0248 (see Figure S5). This corresponds to a Q factor of 18200, determined from $\lambda/\Delta\lambda$ where λ is the cavity mode wavelength and $\Delta\lambda$ the line width of the mode. The broader spectrum which covers the entire spontaneous emission peak is shown in Figure S6, measured with a low-groove density grating of 600 g/mm.

As the excitation power increases beyond the lasing threshold, the line width of the mode

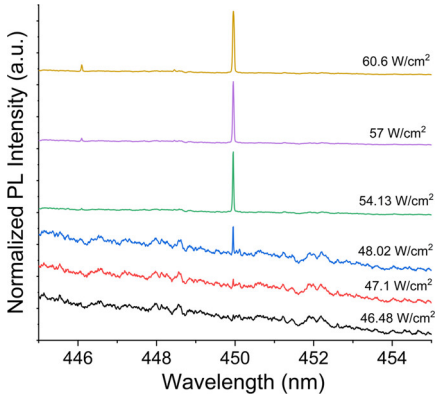

Figure 7: Normalized RT μ-PL spectra below and above the threshold. The y-axis is shifted for clarity.

narrows further, reaching its minimum line width of approximately 0.02 nm, indicating an increase in time coherence of the emitted light in the lasing state. Limited by the optical resolution of the spectrometer of about 0.02 nm, the actual line width might be even narrower. With further increase of the excitation power, the lasing intensity saturates, while the line width increases to ∼0.022 nm, indicating the saturation of gain. When the excitation power exceeds 50 W/cm^2, a second mode begins to appear at the center wavelength of 446.1 nm with a line width of 0.024 nm, although the initial mode remains dominant. With an observed spacing of 3.7 nm between the first and side spectral peak, vertical mode Fabry–Perot (FP) lasing can be ruled out which would otherwise have a spectral spacing in the range of micrometers for microdisk thickness of ∼500 nm. Additionally, for resonant cavities with diameters much larger than their thickness, the Q factor of an FP mode is much lower than that of a WGM as the FP-type Q factor converges to values predicted by the Fresnel equation while the WGM-type Q factors increase without bound.[25] The angle-dependent μ-PL spectra (see Figure S7) indicate that the lasing signal is emitted at a small angle to the in-plane of the disk.

For WGMs of the same order (with the same number of radial and vertical nodes), the free spectral range (FSR) is given by the equation, $\Delta\lambda \sim \lambda^2/(2\pi a_{\text{eff}} n_{\text{eff}})$, where λ is the mode wavelength, a_{eff} is the effective radius of the optical mode, and n_{eff} is the group effective index of refraction. With an observed spacing between two peaks of ∼3.7 nm and a calculated

FSR of ∼2.7 nm (n_{eff} is estimated to be 2.9 at blue regime),[26] it can be deduced that the two observed modes are of different orders (see Figure S8). Figure 8 shows the mode profiles of three types of low-order WGMs in a thin-film microdisk cavity. A first-order WGM without nodes in both the radial and vertical directions is depicted in Figure 8a, while a higher-order (in the vertical direction) WGM is illustrated in Figure 8b, which has no nodes in the radial direction but with two nodes in the vertical direction (WGMs with one node in the vertical direction are not considered due to low overlap with the MQWs in the thin-film microdisk). The mode in Figure 8c is typically termed a higher-order (in the radial direction) WGM, characterized by one node in the radial direction and no nodes in the vertical direction. From the 3D-FDTD simulation results, the mode centered at 449.96 nm is assigned as a first-order mode with $m = 124$, which has no nodes in both the radial and vertical directions. On the other hand, the mode centered at 446.1 nm is assigned as a WGM with $m = 110$, with no nodes in the radial direction but two nodes in the vertical direction. More details of the mode analysis are provided in Supporting Information section 8. Obviously, a_{eff} of the $m110$ WGM is smaller than that of the $m124$ WGM, which could also be seen from the simulated planar electric field distribution maps in Figure 8a,b for the respective modes, where the distance of the electric field antinodes to the centers of the microdisks for the WGM at 446.1 nm is slightly smaller than that of the mode at 449.96 nm. Due to the presence of two nodes in the vertical direction for the mode at 446.1 nm, the overlap factor of this mode is ∼30%, a fraction of that for the 449.96 nm mode.

Multimode lasing is expected for an 8-μm diameter GaN microdisk based on both theory[27] and our previous experimental observations.[10,17–20] However, single-mode lasing is observed under a low excitation power, which remains dominant until it reaches saturation. This is attributed to spatial hole burning (SHB), where the mode with the highest gain depletes all the inverted carriers near the mode's antinodes within the resonant cavity.[28] As a result, although the gain spectrum covers a wide spectral range (see Figure S3), SHB prevents other WGMs ($m = 122, 123, 125$, and 126) from developing, enabling low thresh-

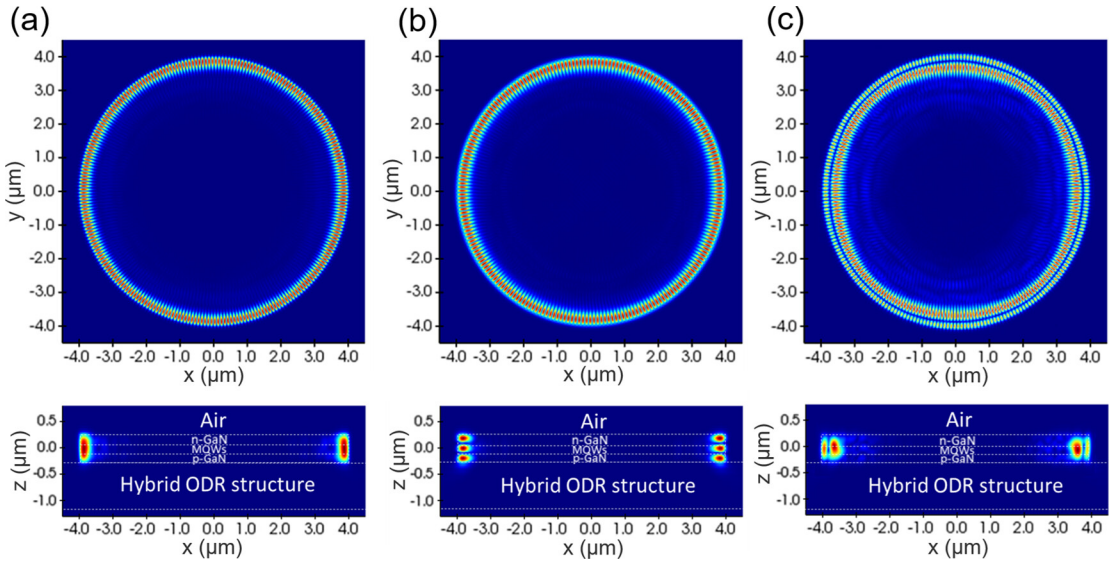

Figure 8: Electric field profiles of three types of low-order WGM from 3D FDTD simulations of 8 μm thin-film microdisks with the hybrid ODR structure: (a) a first-order WGM at 450.28 nm, (b) a higher-order (in the vertical direction) WGM at 446.1 nm, and (c) a higher-order (in the radial direction) WGM at 447.08 nm. The mode field distributions are normalized to their own maximum values, respectively.

old single-mode ($m = 124$) lasing. This phenomenon also underscores both the low optical loss and the strong coupling between the optical mode and the gain region of this proposed structure. Emergence of the second spectral peak at shorter wavelengths at higher excitation powers is commonly attributed to spectral blue-shifting of the InGaN/GaN MQW gain spectra. However, the emission peak of the gain does not exhibit a significant blue-shift (see Figure S9) as measured from an as-prepared thin-film sample due to significantly reduced quantum-confined Stark effect (QCSE) effects from the strain-relaxed thin films.

Compared to the first order WGM near 450 nm ($m = 122, 123, 125$, and 126), the field antinodes of this higher-order WGM with $m = 110$ is located further away from that of the first mode ($m = 124$), leading to an increase in gain. For the second radial order WGM which has a smaller effective radius, besides having much lower Q factor (see Figure S8), its strongest field is further away from the sidewall, resulting in lower out-coupling efficiency compared to the other modes, so that it is not observed in the measured spectra. However, as the excitation power increases, the intensity of the second spectral peak did not strengthen

as rapidly as that of the first peak did. This is attributed to the lower overlap factor of the third vertical order WGM.

Figure 9 presents the lasing threshold as a function of Q factor for 7 microdisk lasers. The lasing threshold ranges from 44 to 56 W/cm^2 (corresponding to the peak threshold powers from 30 to 38 kW/cm^2), while the Q factors vary from 13240 to 18200. The microdisk exhibiting the highest Q factor is picked for detailed analysis in the discussion above. The lasing modes are distributed around the wavelength of 450.5 nm (see Figure S10), aligning well with the center of the MQW emission gain spectrum. This alignment enabled a significant proportion of spontaneous emission to couple into the lasing mode, which also accounts for the low lasing thresholds. From the same figure, a negative correlation between the lasing threshold and the Q factor of the microdisk is observed (through the red dotted line). The fluctuations among devices could be attributed to the slight differences in diameters of the microdisks due to the variations in the dimensions of the silica microspheres, process nonuniformity and defects at the sidewall of GaN microdisks.

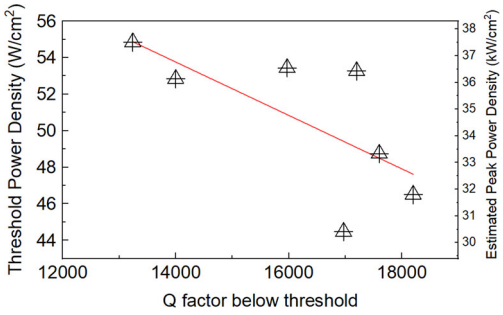

Figure 9: Lasing threshold as a function of the Q factor near threshold.

A summary of key reported figures, including Q factors and lasing threshold, of room temperature optically pumped GaN microdisk lasers are tabulated in Table 1. It is evident that our approach provides the most significant simultaneous enhancement in the Q factor and reduction in lasing threshold. A high Q factor suggests both efficient energy preservation and the effective interaction between the microcavity and the optical mode. In a microdisk laser cavity, the $1/Q$ value, obtained at the emission wavelength, is determined by four primary factors $1/Q = 1/Q_r + 1/Q_a + 1/Q_s + 1/Q_{ex}$. The factor $1/Q_r$ is due to radiation loss

from the disk, $1/Q_a$ is attributed to the optical absorption of the medium, $1/Q_s$ is caused by scattering losses related to surface roughness and other defects, and $1/Q_{ex}$ is ascribed to the energy coupled to the probe. Radiation loss refers to the energy leakage of light during propagation at the interface, and the integration of the hybrid ODR structure in our microdisk plays an important role in minimizing such losses. On the other hand, the smoothness of the top surface of the microdisk laser as observed from the SEM image of Figure 4b, is ensured by the wet etch removal of the Si substrate as compared with thin-film microdisk lasers processed by laser liftoff.[19] Together with the smoothness of the sidewalls, as observed from the SEM image of Figure 4c, scattering losses are minimized. Internal absorption loss is caused by electronic transitions between band edges and defect states. The high dislocation and defect density buffer GaN layer is removed from the thin-film structure to produce a substantial increase in overlap coefficient, which significantly reduces internal absorption loss at the same time. With optimization of all parameters enabled by the thin-film microdisk with ODR combination, the achievement of simultaneous high Q and low threshold lasing is realized.

Conclusions

In this study, we demonstrate a substantial advancement in InGaN MQW microdisk technology, achieving Q factors as high as 18200, while maintaining a low lasing threshold power density of 46.5 W/cm^2 simultaneously. This is achieved through the combination of the thin-film microdisk structure, which provides optimal overlap between the WGMs and the gain layer, and a hybrid ODR that offers high reflectivity across a wide range of angles to promote optical confinement. Using this structure, both critical requirements for attaining a high Q factor and low threshold lasing are satisfied simultaneously. The hybrid-ODR is proven as an effective solution for enhancing the optical confinement of GaN-based microdisks, from both FDTD simulations and experimental measurements.

Funding

This work was supported by a General Research Fund (Project 17205619) sponsored by the Research Grant Council of Hong Kong SAR.

References

(1) Vahala, K. J. Optical microcavities. *Nature* **2003**, *424*, 839–846.

(2) Choi, H. W.; Hui, K. N.; Lai, P. T.; Chen, P.; Zhang, X. H.; Tripathy, S.; Teng, J. H.; Chua, S. J. Lasing in GaN microdisks pivoted on Si. *Applied Physics Letters* **2006**, *89*, 211101.

(3) Kouno, T.; Kishino, K.; Sakai, M. Lasing action on whispering gallery mode of self-organized GaN hexagonal microdisk crystal fabricated by RF-plasma-assisted molecular beam epitaxy. *IEEE Journal of Quantum Electronics* **2011**, *47*, 1565–1570.

(4) Lai, C.-M.; Wu, H.-M.; Huang, P.-C.; Wang, S.-L.; Peng, L.-H. Single-mode stimulated emission from prism-like gallium nitride submicron cavities. *Applied Physics Letters* **2007**, *90*, 141106.

(5) Haberer, E. D.; Sharma, R.; Meier, C.; Stonas, A. R.; Nakamura, S.; DenBaars, S. P.; Hu, E. L. Free-standing, optically pumped, GaN/InGaN microdisk lasers fabricated by photoelectrochemical etching. *Applied Physics Letters* **2004**, *85*, 5179–5181.

(6) Tamboli, A. C.; Haberer, E. D.; Sharma, R.; Lee, K. H.; Nakamura, S.; Hu, E. L. Room-temperature continuous-wave lasing in GaN/InGaN microdisks. *Nature Photonics* **2007**, *1*, 61–64.

(7) Simeonov, D.; Feltin, E.; Bühlmann, H. J.; Zhu, T.; Castiglia, A.; Mosca, M.; Carlin, J.-F.; Butte, R.; Grandjean, N. Blue lasing at room temperature in high quality factor

GaN/AlInN microdisks with InGaN quantum wells. *Applied Physics Letters* **2007**, *90*, 061106.

(8) Simeonov, D.; Feltin, E.; Altoukhov, A.; Castiglia, A.; Carlin, J.-F.; Butte, R.; Grandjean, N. High quality nitride based microdisks obtained via selective wet etching of AlInN sacrificial layers. *Applied Physics Letters* **2008**, *92*, 171102.

(9) Aharonovich, I.; Woolf, A.; Russell, K. J.; Zhu, T.; Niu, N.; Kappers, M. J.; Oliver, R. A.; Hu, E. L. Low threshold, room-temperature microdisk lasers in the blue spectral range. *Applied Physics Letters* **2013**, *103*, 021112.

(10) Zhang, X.; Cheung, Y. F.; Zhang, Y.; Choi, H. W. Whispering-gallery mode lasing from optically free-standing InGaN microdisks. *Optics Letters* **2014**, *39*, 5614–5617.

(11) Athanasiou, M.; Smith, R.; Liu, B.; Wang, T. Room temperature continuous–wave green lasing from an InGaN microdisk on silicon. *Scientific Reports* **2014**, *4*, 7250.

(12) Selles, J.; Crepel, V.; Roland, I.; Kurdi, M. E.; Checoury, X.; Boucaud, P.; Mexis, M.; Leroux, M.; Damilano, B.; Rennesson, S.; Semond, F. III-Nitride-on-silicon microdisk lasers from the blue to the deep ultra-violet. *Applied Physics Letters* **2016**, *109*, 231101.

(13) Tabataba-Vakili, F.; Brimont, C.; Alloing, B.; Damilano, B.; Doyennette, L.; Guillet, T.; Kurdi, M. E.; Chenot, S.; Brändli, V.; Frayssinet, E.; Duboz, J.-Y.; Semond, F.; Gayral, B.; Boucaud, P. Analysis of low-threshold optically pumped III-nitride microdisk lasers. *Applied Physics Letters* **2020**, *117*, 121103.

(14) Mei, Y.; Xie, M.; Long, H.; Ying, L. Y.; Zhang, B. P. Low threshold GaN-based microdisk lasers on silicon with high Q factor. *Journal of Lightwave Technology* **2022**, *40*, 2952–2958.

(15) Amano, H.; Sawaki, N.; Akasaki, I.; Toyoda, Y. Metalorganic vapor phase epitaxial

growth of a high quality GaN film using an AlN buffer layer. *Applied Physics Letters* **1986**, *48*, 353–355.

(16) Pal, S.; Jacob, C. Silicon—a new substrate for GaN growth. *Bulletin of Materials Science* **2004**, *27*, 501–504.

(17) Zi, H.; Fu, W. Y.; Tabataba-Vakili, F.; Kim-Chauveau, H.; Frayssinet, E.; Mierry, P. D.; Damilano, B.; Duboz, J.-Y.; Boucaud, P.; Semond, F.; Choi, H. W. Whispering-gallery mode InGaN microdisks on GaN substrates. *Optics Express* **2021**, *29*, 21280–21289.

(18) Zi, H.; Fu, W. Y.; Cheung, Y. F.; Damilano, B.; Frayssinet, E.; Alloing, B.; Duboz, J.-Y.; Boucaud, P.; Semond, F.; Choi, H. W. Comparison of lasing characteristics of GaN microdisks with different structures. *Journal of Physics D: Applied Physics* **2022**, *55*, 355107.

(19) Zi, H.; Cheung, Y. F.; Damilano, B.; Frayssinet, E.; Alloing, B.; Duboz, J.-Y.; Boucaud, P.; Semond, F.; Choi, H. W. Influence of surface roughness on the lasing characteristics of optically pumped thin-film GaN microdisks. *Optics Letters* **2022**, *47*, 1521–1524.

(20) Fu, W. Y.; Cheung, Y. F.; Choi, H. W. Monolithic multi-wavelength lasing from multi-sized microdisk lasers. *Optics Letters* **2022**, *47*, 6397–6400.

(21) Chen, C.-C.; Shih, M.-H.; Yang, Y.-C.; Kuo, H.-C. Ultraviolet GaN-based microdisk laser with AlN/AlGaN distributed Bragg reflector. *Applied Physics Letters* **2010**, *96*, 151115.

(22) Shakya, J.; Knabe, K.; Kim, K. H.; Li, J.; Lin, J. Y.; Jiang, H. X. Polarization of III-nitride blue and ultraviolet light-emitting diodes. *Applied Physics Letters* **2005**, *86*, 091107.

(23) Gao, B.; George, J. P.; Beeckman, J.; Neyts, K. Design, fabrication and characterization of a distributed Bragg reflector for reducing the étendue of a wavelength converting system. *Optics Express* **2020**, *28*, 12837–12846.

(24) Selhofer, H.; Ritter, E.; Linsbod, R. Properties of titanium dioxide films prepared by reactive electron-beam evaporation from various starting materials. *Applied Optics* **2002**, *41*, 756–762.

(25) Baek, H.; Hyun, J. K.; Chung, K.; Oh, H.; Yi, G. C. Selective excitation of Fabry–Perot or whispering-gallery mode-type lasing in GaN microrods. *Applied Physics Letters* **2014**, *105*, 201108.

(26) Jr., A. S. B.; Ilegems, M. Infrared lattice vibrations and free-electron dispersion in GaN. *Physical Review B* **1973**, *7*, 743–750.

(27) Numai, T. *Fundamentals of Semiconductor Lasers*, 2nd ed.; Springer Series in Optical Sciences; Springer Japan, 2015.

(28) Siegman, A. E. *Lasers*; University Science Books: Mill Valley, CA, 1986.

(29) Zhu, G.; Li, J.; Zhang, N.; Li, X.; Dai, J.; Cui, Q.; Song, Q.; Xu, C.; Wang, Y. Whispering-Gallery Mode Lasing in a Floating GaN Microdisk with a Vertical Slit. *Scientific Reports* **2020**, *10*, 253.

Table 1: Comparison of Lasing Characteristics of an Optical Pumping Microdisk at RT.

Reference	d (μm)	excitation source	λ (nm)	threshold energy density	avg. threshold power density	Q factor below/above threshold	estimated peak threshold power density
Haberer et al.[5]	3.5	193 nm, 50 Hz, 9 ns	418.2	–	12.1 W/cm^2	–/4647	26.9 MW/cm^2
Tamboli et al.[6]	1.2	325 nm CW	428	–	300 W/cm^2	3700/–	300 W/cm^2
Simeonov et al.[7]	4	266 nm, 500 ps, 8 kHz	422.5	–	>1.5 W/cm^2	4000/12800	400 kW/cm^2
Simeonov et al.[8]	5	244 nm CW	408.8	–	166 kW/cm^2	3500/12388	166 kW/cm^2
Chen et al.[21]	4.7	355 nm, 0.5 ns, 1 kHz	377	–	30 W/cm^2	400/–	60 MW/cm^2
Aharonovich et al.[9]	1	380 nm, 200 ps, 76 MHz	475.8	0.28 mJ/cm^2	–	2162/6600	1.4 MW/cm^2
Zhang et al.[10]	6.6	349 nm, 4 ns, 1 kHz	430.2	8.42 mJ/cm^2	–	770/–	2.1 MW/cm^2
Athanasiou et al.[11]	1	405 nm CW	514	–	1000 W/cm^2	2150/3023	1 kW/cm^2
Selles et al.[12]	3	266 nm, 400 ps, 4 kHz	275	15 mJ/cm^2	–	4000/–	37.5 MW/cm^2
Selles et al.[12]	4	266 nm, 400 ps, 4 kHz	417	3 mJ/cm^2	–	2500/–	7.5 MW/cm^2
Zhu et al.[29]	9	355 nm, 6 ns, 10 Hz	377.3	–	180 kW/cm^2	–/1300	180 kW/cm^2
Tabataba–Vakili et al.[13]	3	355 nm, 4 ns, 7 kHz	419	0.07 mJ/cm^2	–	6000/–	18 kW/cm^2
Zi et al.[17]	8	349 nm, 4 ns, 1 kHz	436.8	5.2 mJ/cm^2	–	3000/–	1.3 MW/cm^2
Zi et al.[18]	8	349 nm, 4 ns, 1 kHz	455.3	2.1 mJ/cm^2	–	4200/–	525 kW/cm^2
Zi et al.[19]	8	349 nm, 4 ns, 1 kHz	452	2.9 mJ/cm^2	–	3100/–	725 kW/cm^2
Fu et al.[20]	10	349 nm, 4 ns, 1 kHz	516.9	5.3 mJ/cm^2	–	4308/–	1.33 MW/cm^2
Mei et al.[14]	28	355 nm	412.9	33.6	–	12543/–	33.6